DUST DYNAMICS, SURFACE BRIGHTNESS PROFILES, AND THERMAL SPECTRA OF DEBRIS DISKS: THE CASE OF AU MICROSCOPII

Linda E. Strubbe[1] and Eugene I. Chiang[1,2]

ABSTRACT

AU Microscopii is a 12 Myr old M dwarf that harbors an optically thin, edge-on disk of dust. The scattered light surface brightness falls with projected distance b from the star as $b^{-\alpha}$; within $b = 43$ AU, $\alpha \approx 1$–2, while outside 43 AU, $\alpha \approx 4$–5. We devise a theory to explain this profile. At a stellocentric distance $r = r_{BR} = 43$ AU, we posit a ring of parent bodies on circular orbits: the "birth ring," wherein micron-sized grains are born from the collisional attrition of parent bodies. The "inner disk" at $r < r_{BR}$ contains grains that migrate inward by corpuscular and Poynting-Robertson (CPR) drag. The "outer disk" at $r > r_{BR}$ comprises grains just large enough to remain bound to the star, on orbits rendered highly eccentric by stellar wind and radiation pressure. How the vertical optical depth $\tau_\perp$ scales with r depends on the fraction of grains that migrate inward by CPR drag without suffering a collision. If this fraction is large, the inner disk and birth ring share the same optical depth, and $\tau_\perp \propto r^{-5/2}$ in the outer disk. By contrast, under collision-dominated conditions, the inner disk is empty, and $\tau_\perp \propto r^{-3/2}$ outside. These scaling relations, which we derive analytically and confirm numerically, are robust against uncertainties in the grain size distribution. By simultaneously modeling the surface brightness and thermal spectrum, we break model degeneracies to establish that the AU Mic system is collision dominated and that its narrow birth ring contains a lunar mass of decimeter-sized bodies. The inner disk is devoid of micron-sized grains; the surface brightness at $b \lesssim 43$ AU arises from light forward scattered by the birth ring. Inside $b = 43$ AU, the disk's $V - H$ color should not vary with b; outside, the disk must become bluer as ever smaller grains are probed.

Subject headings: accretion, accretion disks — celestial mechanics — circumstellar matter — planetary systems: formation — stars: individual (AU Mic) — stars: mass loss

1. INTRODUCTION

"Debris disks" surrounding young stars are composed of optically thin dust (see the reviews by Artymowicz 2000; Lagrange et al. 2000; Zuckerman 2001). Most debris disks are inferred to exist from measurements of infrared excesses (e.g., Aumann et al. 1984; Habing et al. 2001; Zuckerman & Song 2004). A few disks are close enough to resolve in images, either in scattered starlight (e.g., Smith & Terrile 1984; Schneider et al. 1999; Kalas et al. 2005) or in thermal emission (e.g., Telesco et al. 2000; Greaves et al. 2004).

Is the observed dust primordial—the remains of an optically thick, gas-rich disk from a previous Herbig Ae or T Tauri phase? Or is it maintained in equilibrium, continuously removed by processes such as Poynting-Robertson drag and replenished by the comminution of larger, colliding parent bodies? A third possibility is that the observed dust represents the transient aftermath of recent cataclysmic events. Dust might be freshly generated, unequilibrated debris from the catastrophic destruction of large planetesimals (Su et al. 2005; Song et al. 2005).

The debris disk encircling the young M dwarf AU Microscopii is a promising place to investigate these questions. It is well resolved in scattered light from optical to near-infrared wavelengths (Kalas et al. 2004; Krist et al. 2005, hereafter K05; Liu 2004; Metchev et al. 2005). Of central relevance to our study is the disk's surface brightness profile. Within a projected distance b from the star of 43 AU, the surface brightness SB falls approximately as $b^{-1.8}$ (K05). We refer to this region as the "inner disk." Outside 43 AU, in the "outer disk," the slope of the profile changes dramatically: SB $\propto b^{-4.7}$ (K05). This break is observed independently by other researchers (Liu 2004; Metchev et al. 2005). The shape of the profile is all the more significant because it resembles that of the debris disk surrounding β Pictoris (Kalas & Jewitt 1995; Liu 2004) and of the recently discovered disk encompassing HD 139664 (Kalas et al. 2006). AU Mic's disk is also detected in unresolved thermal emission (Liu et al. 2004; Chen et al. 2005). The disk's infrared spectrum peaks at a wavelength of ~ 100 μm and exhibits no excess at 12 μm; this behavior suggests that the disk contains an inner hole (Liu et al. 2004).

Here we offer a theory that explains these observations quantitatively. The reason why the surface brightness profile breaks at 43 AU is that a narrow ring of parent bodies, analogous to the solar system's Kuiper Belt, orbits the star at a stellocentric radius $r = r_{BR} = 43$ AU. The subscript "BR" refers to our term for the belt of parent bodies, the "birth ring," wherein micron-sized dust grains are born through collisions of larger planetesimals. Grain creation is balanced in steady state by destructive grain-grain collisions and removal by corpuscular and Poynting-Robertson (CPR) drag.[3] Corpuscular drag exerted by the young M dwarf's wind is probably at least a few times more effective at removing dust than Poynting-Robertson drag in the AU Mic system, a possibility first pointed out by Plavchan et al. (2005, hereafter PJL05). The outer disk comprises grains that are only tenuously bound, moving on orbits rendered highly eccentric by stellar wind and radiation forces (e.g., Lecavelier des Etangs et al. 1996; Augereau et al. 2001). These barely bound grains dominate

---

[1] Center for Integrative Planetary Sciences, Astronomy Department, University of California at Berkeley, Berkeley, CA 94720; linda@astron.berkeley.edu, echiang@astron.berkeley.edu.
[2] Alfred P. Sloan Research Fellow.

[3] Our analysis ignores any gas that might still be orbiting the star. Only upper limits are observed for the column of gas toward the star: $N_{H_2} < 1.7 \times 10^{19}$ cm^{-2} (Roberge et al. 2005).

scattering of starlight in the outer disk. By contrast, unbound grains escape the system too quickly for their steady-state population to contribute appreciably to the surface brightness. The inner disk is populated by grains that migrate inward by CPR drag quickly enough to evade collisional destruction. In CPR-dominated (what we refer to as "type A") disks, a large fraction of grains meets this condition, unlike in collision-dominated ("type B") disks. Similar classifications were put forward by Wyatt (2005) and Meyer et al. (2006) in their considerations of disks composed of single-sized grains. We calculate simultaneously the steady-state spatial and size distributions of dust particles and derive how the outer disk's optical depth scales with radius for type A and type B disks. Our analysis accounts for destructive grain-grain collisions and the detailed dynamics of CPR drag, which reduces not only the orbital semimajor axes of grains but also their orbital eccentricities (Wyatt & Whipple 1950). The reduction of orbital eccentricity is not often considered but is a key component of our theory. Whether type A or type B conditions apply to AU Mic's disk is determined in part by the strength of the stellar wind, which according to previous works is uncertain by orders of magnitude. In this work we place a novel constraint on the stellar mass-loss rate and decide the appropriate disk type by comparing our theoretical models to the observations.

In § 2 we lay down basic parameters of the AU Mic system: stellar properties, disk optical depths, timescales for grain-grain collisions, and how the star's wind and radiation alter orbits of dust grains. In § 3 we employ order-of-magnitude physics and analytic scalings to understand how the interplay between collisions, blowout, and drag shapes the observed surface brightness profiles of the inner and outer disks. There we derive the steady-state grain size distribution as a function of position, including the maximum sizes and total mass of parent bodies. In § 4 we verify and extend our analytic results with a Monte Carlo simulation of the disk's surface brightness, color, and spectral energy distribution (SED). Models are compared directly with observations. Finally, in § 5 we summarize our theory, place it in context with our understanding of how planets form, and point out directions for future research.

2. PRELIMINARIES

We establish orders of magnitude characterizing the AU Mic system. Stellar properties, including the stellar mass-loss rate that figures prominently throughout our analysis, are reviewed in § 2.1. Collision times between grains and relative collision velocities are estimated in § 2.2. Grain dynamics relevant to our theory include blowout by stellar wind and radiation pressure, as discussed in § 2.3, and orbital decay by corpuscular and Poynting-Robertson drag, as treated in § 2.4.

2.1. Stellar Properties

AU Microscopii is a spectral type dM1e star located a distance $d = 9.9$ pc from Earth. It has mass $M_* = 0.5 \, M_\odot$, radius $R_* = 0.93 \, R_\odot$, effective temperature $T_* = 3500$ K, luminosity $L_* = 0.1 \, L_\odot$, V magnitude 8.8, and H magnitude 4.8 (Kalas et al. 2004; Metchev et al. 2005 and references therein). The star's age is estimated to be $t_{age} = 12^{+8}_{-4}$ Myr. AU Mic's X-ray luminosity is a prodigious $L_X = 5.5 \times 10^{29}$ ergs s^{-1} = $3 \times 10^{-3} L_*$ (Hünsch et al. 1999). The star flares at both X-ray and ultraviolet wavelengths (Magee et al. 2003). The stellar rotation period is 4.87 days (Torres & Ferraz Mello 1973).

How strong is AU Mic's stellar wind? The wind velocity v_{wind} is likely of order the stellar escape velocity $v_{esc} = (2GM_*/R_*)^{1/2} \approx$

450 km s^{-1}. PJL05 discuss what is known about mass-loss rates $\dot{M}_*$ from M dwarfs, citing values ranging from 10 to as high as 10^4 times the solar mass-loss rate of $\dot{M}_\odot = 2 \times 10^{-14} \, M_\odot$ yr^{-1}. While the star's youth, flaring activity, and fast rotation suggest that a powerful wind emanates from AU Mic, the star's X-ray emission indicates otherwise. Wood et al. (2002, 2005) study the relationship between X-ray luminosity and stellar mass-loss rate by measuring $\dot{M}_*$ from a handful of M, K, and G dwarfs having ages $\gtrsim 500$ Myr. They establish that the mass flux at the stellar surface $F_M \equiv \dot{M}_*/(4\pi R_*^2)$ increases with X-ray surface flux $F_X \equiv L_X/(4\pi R_*^2)$ for $F_X < 8 \times 10^5$ ergs cm^{-2} s^{-1} $\equiv F_{X, crit}$. The mass flux F_M saturates at a maximum of $10^2 F_{M,\odot}$. For $F_X > F_{X, crit}$, F_M drops to $\lesssim 10 F_{M,\odot}$, perhaps because the strong magnetic fields of such extraordinarily X-ray–active stars inhibit stellar winds (see also Schrijver & Title 2001; Strassmeier 2002). AU Mic's X-ray flux $F_X \sim 1 \times 10^7$ ergs cm^{-2} s^{-1} exceeds $F_{X, crit}$, implying at face value a relatively low mass-loss rate. Nevertheless, it is unclear whether the measurements of Wood et al. (2005) apply to this highly variable, pre–main-sequence star. To accommodate the uncertainty in AU Mic's mass-loss rate, we consider in our analysis a wide range of values, $\dot{M}_* \in (1, \, 10, \, 10^2, \, 10^3) \dot{M}_\odot$. We ultimately find in § 4 that detailed comparison between theoretical models of the disk and observations can, in fact, constrain $\dot{M}_*$.

2.2. Collision Times

Consider for the moment a disk of single-sized particles on low-eccentricity orbits. Where the vertical, geometric optical depth equals $\tau_\perp$, the mean free time between collisions is

$$t_c \sim \frac{1}{\Omega \tau_\perp}, \qquad (1)$$

where Ω is the local orbital angular frequency. This expression may be derived by recognizing that every $\sim 1/\Omega$ orbital period, a typical particle traverses an optical depth of $\sim \tau_\perp$ over the course of its vertical epicycle. For $\tau_\perp < 1$, the particle collides with probability $\tau_\perp$; for $\tau_\perp > 1$, it undergoes $\tau_\perp$ collisions per orbit.

Detailed fits to observations in § 4 reveal that the total vertical, geometric optical depth in the birth ring at $r = r_{BR} = 43$ AU equals $\tau_{\perp, BR} \equiv \tau_\perp(r_{BR}) = 4 \times 10^{-3}$. We define a fiducial collision time

$$t_{c, BR} \equiv \frac{1}{\Omega \tau_{\perp, BR}} \sim 2 \times 10^4 \left(\frac{4 \times 10^{-3}}{\tau_{\perp, BR}} \right) \text{ yr}. \qquad (2)$$

The collision lifetime $t_{col}(s)$ is the time a grain of radius s survives before it is destroyed by colliding with another grain. Unlike the case for t_c, in calculating t_{col} we do not assume that particles have a single size. For a given collisional specific energy Q^* (ergs g^{-1}; Greenberg et al. 1978; Fujiwara et al. 1989), targets of size s suffer catastrophic dispersal by smaller projectiles of minimum size

$$s_{proj} \sim \left(\frac{2Q^*}{v_{rel}^2} \right)^{1/3} s$$
$$\sim 0.6 \left(\frac{Q^*}{10^7 \text{ ergs g}^{-1}} \right)^{1/3} \left(\frac{100 \text{ m s}^{-1}}{v_{rel}} \right)^{2/3} s, \qquad (3)$$

which is comparable to s. By catastrophic dispersal we mean that the mass of the largest postcollision fragment is no greater than half the mass of the original target and that collision fragments disperse without gravitational reassembly. We have normalized

$\dot{M}_*/\dot{M}_\odot$	$P_{\rm SWR}$	$P_{\rm CPR}$	$s_{\rm blow}$[a] (μm)	$t_{\rm CPR}(s = 1.1s_{\rm blow})$[b] (yr)	$t_{\rm CPR}(s = 1.5s_{\rm blow})$[b] (yr)	$t_{\rm CPR}(s = 15s_{\rm blow})$[b] (yr)
1..................................	2.0	5.0	0.23	9.5×10^6	4.9×10^6	1.9×10^7
10................................	2.0	32	0.23	1.5×10^6	7.8×10^5	3.1×10^6
10^2	2.4	3.0×10^2	0.28	1.9×10^5	9.9×10^4	3.9×10^5
10^3	6.4	3.0×10^3	0.74	5.1×10^4	2.6×10^4	1.0×10^5

NOTE.—Assumes $Q_{\rm rad} = 2$, $Q_{\rm wind} = 1$, $\rho = 2$ g cm^{-3}, $v_{\rm wind} = 450$ km s^{-1}, $L_* = 0.1\,L_\odot$, $M_* = 0.5\,M_\odot$, $\dot{M}_\odot = 2 \times 10^{-14}\,M_\odot$ yr^{-1}, and $r_{\rm peri} = r_{\rm BR} = 43$ AU.

[a] The blowout radius is such that $\beta = \frac{1}{2}$.

[b] Calculated for $e = e_0$. For $s/s_{\rm blow} = \{1.1,\ 1.5,\ 15\}$, $e_0 = \{0.83,\ 0.50,\ 0.034\}$ by eqs. (9a)–(9c) and $E(e_0) = \{7.2,\ 2.7,\ 1.1\}$ by eq. (14).

the relative speed $v_{\rm rel}$ to the vertical velocity dispersion of visible grains at $r = r_{\rm BR} = 43$ AU,

$$\Omega \frac{h_{\rm BR}}{2} \sim 100 \text{ m s}^{-1}, \tag{4}$$

where the full vertical disk height $h_{\rm BR} \approx 2.75$ AU (K05). We have normalized Q^* to a value appropriate for centimeter-sized silicate targets (Greenberg et al. 1978; Fujiwara et al. 1989). Ice targets of similar size have specific energies that are 2 orders of magnitude smaller (Greenberg et al. 1978). On the other hand, it is possible that Q^* increases with decreasing size (Fujiwara et al. 1989; Housen & Holsapple 1990), perhaps as fast as $Q^* \propto s^{-0.5}$. If so, grains having sizes $s \sim 1$ μm would be $\sim$100 times stronger than their centimeter-sized counterparts, thereby possibly canceling the reduction in strength due to an icy composition. To keep the telling of our story as simple as possible, we adhere to a nominal, size-independent value of $Q^* = 10^7$ ergs g^{-1}. The essential point is that collisions between comparably sized grains in the AU Mic disk are destructive.[4]

2.3. Blowout by Stellar Wind and Radiation Pressure

Grains of certain sizes cannot occupy orbits bound to the star because of stellar wind and radiation (SWR) forces. The ratio of repulsive to gravitational forces felt by a grain equals

$$\beta = \frac{F_{\rm rad} + F_{\rm wind}}{F_{\rm grav}} \tag{5}$$

$$= \frac{3}{16\pi} \frac{L_* P_{\rm SWR}}{G M_* c \rho s}, \tag{6}$$

where the dimensionless factor

$$P_{\rm SWR} \equiv Q_{\rm rad} + Q_{\rm wind} \frac{\dot{M}_* v_{\rm wind} c}{L_*} \tag{7}$$

measures the extent to which the ram pressure exerted by the (assumed radial) wind dominates radiation pressure.[5] Here s and $\rho \sim 2$ g cm^{-3} are, respectively, the radius and internal density of a particle, G is the gravitational constant, c is the speed of light,

---

[4] Commercial sandblasting machines accelerate abrasive particles up to speeds of 100 m s^{-1}.

[5] The assumption of a purely radial wind is valid insofar as the azimuthal velocity of the wind $v_{\rm wind,\phi}$ is less than Ωr. By modeling the stellar magnetic field as that of a rotating (split) monopole (Weber & Davis 1967; Parker 1964), we estimate that $v_{\rm wind,\phi}/\Omega r \lesssim 1/30$.

$Q_{\rm rad} \lesssim 2$ is the cross section that the grain presents to radiation pressure in units of the geometric cross section (Burns et al. 1979), and $Q_{\rm wind} \sim 1$ is the analogous dimensionless cross section the grain presents to wind pressure.[6] For $Q_{\rm rad} \sim 2$ (appropriate for the $s > \lambda_*/2\pi$ geometric optics limit, where $\lambda_* \approx 1$ μm is the wavelength at which the bulk of the stellar luminosity is emitted), wind pressure is negligible compared to radiation pressure except for the largest value of $\dot{M}_*$ considered. Table 1 lists possible values for $P_{\rm SWR}$.

Grains are continually created from colliding parent bodies. Throughout this paper we assume that parent bodies move on nearly circular ($\beta \ll 1$) orbits and that the velocities with which grains are ejected from parent bodies are small compared to parent body orbital velocities. These assumptions imply that grains having $\beta \geq \frac{1}{2}$ are "blown out" by SWR pressure. For constant $P_{\rm SWR}$ with s, the condition $\beta \geq \frac{1}{2}$ is equivalent to

$$s \leq s_{\rm blow} = \frac{3}{8\pi} \frac{L_* P_{\rm SWR}}{G M_* c \rho} \sim 0.2 \left(\frac{P_{\rm SWR}}{2}\right) \mu\text{m}. \tag{8}$$

Grains for which $s < s_{\rm blow}$ are unbound and move on hyperbolic escape trajectories. Grains for which $s = s_{\rm blow}$ move on parabolic escape trajectories. A grain for which $s - s_{\rm blow} \ll s_{\rm blow}$ moves initially on a highly elliptical orbit whose periastron distance $r_{\rm peri,0}$ equals the orbital radius of the parent body. It is these "barely bound" grains that contribute significantly to the scattered light observed in the outer disk. The initial eccentricity e_0 and semimajor axis a_0 of a barely bound grain upon its birth are uniquely related to grain size s via the force ratio β:

$$e_0 = \frac{\beta}{1 - \beta}, \tag{9a}$$

$$a_0 = \frac{r_{\rm peri,0}}{1 - e_0}, \tag{9b}$$

$$\beta = \frac{1}{2} \left(\frac{s_{\rm blow}}{s}\right), \tag{9c}$$

where the last relation assumes that $P_{\rm SWR}$ is independent of s.

A consequence of equations (1) and (9a)–(9c) is that grains on highly eccentric orbits have prolonged collision times. Provided that the optical depth traversed by a grain is concentrated near periastron at $r = r_{\rm peri}$, the optical depth $\tau_\perp$ in equation (1) should be evaluated at $r = r_{\rm peri}$. However, Ω should not necessarily be

---

[6] Our $Q_{\rm rad}$ equals $Q_{\rm pr}$ from Burns et al. (1979). It should not be confused with $Q_{\rm scat}$, the usual scattering efficiency.

evaluated for a semimajor axis equal to $r_{\rm peri}$. Instead, from equation (9b),

$$\Omega(e) = \left(\frac{GM_*}{r_{\rm peri}^3}\right)^{1/2} (1-e)^{3/2}. \tag{10}$$

A related useful quantity is the fraction of time a grain on a fixed orbit spends at radii between $r_{\rm peri}$ and $r_{\rm peri} + \Delta r$:

$$f(e) \sim \left(\frac{\Delta r}{r_{\rm peri}}\right)^{1/2} \frac{(1-e)^{3/2}}{(1+e)^{1/2}}, \tag{11}$$

valid in the limit of $\Delta r \ll r_{\rm peri}$ and large e.

2.4. Corpuscular and Poynting-Robertson Drag

Under the drag due to CPR forces (see, e.g., Burns et al. 1979), dust grain orbits having periastron distances $r_{\rm peri}$ and arbitrary eccentricities e collapse to a point in a time

$$t_{\rm CPR} = \frac{4\pi c^2 \rho}{3 L_* P_{\rm CPR}} E(e) r_{\rm peri}^2 s, \tag{12}$$

where the dimensionless factor

$$P_{\rm CPR} \equiv Q_{\rm rad} + Q_{\rm wind} \frac{\dot{M}_* c^2}{L_*} \tag{13}$$

quantifies the relative importance of wind-driven versus radiation-driven drag. For the values of $\dot{M}_*$ we consider, the stellar wind is at least as important as the stellar radiation: $P_{\rm CPR} > 2$ (see Table 1). The dimensionless factor

$$E(e) = \frac{8}{5} \frac{(1+e)^2}{e^{8/5}} \int_0^e \frac{x^{3/5} dx}{(1-x^2)^{3/2}} \tag{14}$$

governs the decay of orbital eccentricity (Wyatt & Whipple 1950). A related useful result from Wyatt & Whipple (1950) is that

$$\frac{de}{dt} = \left(\frac{15 L_* P_{\rm CPR}}{32 \pi c^2 \rho r_{\rm peri,0}^2}\right) \frac{1}{s} \frac{e_0^{8/5}}{(1+e_0)^2} \frac{(1-e^2)^{3/2}}{e^{3/5}}. \tag{15}$$

The initial effect of CPR drag on a highly eccentric orbit is to reduce the apastron distance while keeping the periastron distance and eccentricity nearly fixed (see Fig. 1 of Wyatt & Whipple 1950). For highly eccentric orbits, the time spent during this apastron reduction phase is much longer than the usual CPR timescales that are cited for $e \ll 1$. As e approaches 1, E diverges as

$$E(e \approx 1) \propto (1-e)^{-1/2}. \tag{16}$$

Once CPR drag reduces the eccentricity to values less than a few percent, the entire orbit collapses to a point in a time given by $t_{\rm CPR}$ with $E \approx 1$.

Table 1 provides sample values of $t_{\rm CPR}(e = e_0)$ for three choices of $s/s_{\rm blow} = \{1.1, 1.5, 15\}$, while Figure 1 depicts how $t_{\rm CPR}(e = e_0)$ varies with s, all for $r_{\rm peri} = r_{\rm BR} = 43$ AU.

3. THEORY

We assemble the ingredients laid out in § 2 into a theory for the distribution of grain sizes (§ 3.1) and the profile of optical
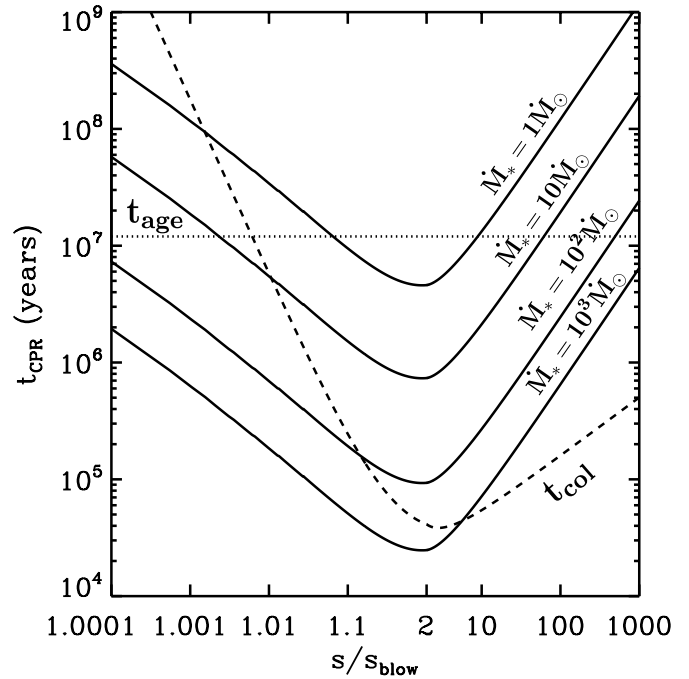

Fig. 1.—CPR drag time as a function of grain size $s/s_{\rm blow}$, for $\dot{M}_*/\dot{M}_\odot = \{1, 10, 10^2, 10^3\}$. To highlight the behavior as $s \to s_{\rm blow}$, the horizontal axis is scaled as $\log(s/s_{\rm blow} - 1)$. The fiducial collision time $t_{\rm col} = t_{c, \rm BR}(s/s_{\rm blow})^{1/2} \times (1 - e_0)^{-3/2}$ is also indicated as a dashed line (see § 3.1.3). The size $s_{\rm break}$ corresponds approximately to where this collision time and the CPR drag time are equal. Timescales for removal by CPR drag and collisions can be much shorter than the age of the system, $t_{\rm age}$.

depth (§ 3.2) in the AU Mic disk. Included in our analysis are estimates of the sizes and total mass of the largest parent bodies undergoing a collisional cascade. According to our theory, all of the current optical to near-IR observations probe grains whose population is maintained in steady state and that are still bound (most only barely) to the central star. Contributions to scattered light from unbound and unequilibrated populations of grains are assessed in §§ 3.3 and 3.4, respectively.

3.1. Equilibrium Size Distribution

We posit an annulus of parent bodies extending from $r = r_{\rm BR} - \Delta r/2$ to $r = r_{\rm BR} + \Delta r/2$—the "birth ring"—where grains are born from the collisional attrition of larger parent bodies. These grains travel on orbits whose eccentricities and semimajor axes are continuously modified by CPR drag. Grains are removed from the birth ring either by CPR drag or by collisions with other grains. The goal of this section is to determine the equilibrium size distribution dN/ds as a function of r, where dN is the vertical column density of grains having sizes between s and $s + ds$.

The size distribution of dust in debris disks is commonly assumed to be proportional to $s^{-q_{\rm ce}} = s^{-7/2}$. This scaling is appropriate for grains on low-eccentricity orbits whose collisional strengths are independent of size, whose spatial distribution is homogeneous, and whose numbers are maintained in a purely collisional equilibrium, as first derived by Dohnanyi (1969; see also O'Brien & Greenberg 2003; Pan & Sari 2005). In such equilibrium cascades, as much mass is ground into every size bin as is ground out. One presumption behind the cascade is that collision times are short enough that the system has relaxed into collisional equilibrium. However, Figure 1 shows that $t_{\rm CPR}$ and $t_{\rm col}$ are of the same order for some grain sizes. Visible dust may

be removed too quickly by CPR drag to participate in a purely collisional, equilibrium cascade.

Instead of making the usual assumption that the size distribution is proportional to $s^{-7/2}$ for all s, we construct the following model. We define s_{break} as the radius of the grain for which

$$t_{\mathrm{col}}(s_{\mathrm{break}}) = t_{\mathrm{CPR}}(s_{\mathrm{break}}) \qquad (17)$$

at $r = r_{\mathrm{BR}}$. We expect that grains of a given size can participate in a standard collisional cascade if they have had enough time to collide destructively about once (for numerical estimates of the time required for a cascade to equilibrate see, e.g., Campo Bagatin et al. 1994 and references therein). For $s > s_{\mathrm{break}}$, we expect $t_{\mathrm{CPR}} > t_{\mathrm{col}}$ and a Dohnanyi-like size distribution (modified appropriately for grains on highly eccentric orbits, i.e., for spatial inhomogeneity). For $s < s_{\mathrm{break}}$, we will see that $t_{\mathrm{CPR}} < t_{\mathrm{col}}$. The two regimes are treated in §§ 3.1.2 and 3.1.1, respectively. We discuss which grain sizes carry the bulk of the optical depth and how collision times vary with grain size in § 3.1.3. These considerations are applied to computing s_{break} in § 3.1.4. The sizes of the largest parent bodies are estimated in § 3.1.5.

Readers interested only in our results for the grain size distribution can examine equations (18), (21), (23), (25), (26), (27), (37), and (39) and can skip ahead to § 3.2, where grain dynamics are analyzed.

3.1.1. Equilibrium Size Distribution for $s < s_{\mathrm{break}}$

First, we define

$$\frac{d\mathcal{N}}{ds} \equiv \int_0^\infty \frac{dN}{ds} 2\pi r \, dr \qquad (18)$$

as the size distribution of grains integrated over the entire disk.

Fresh debris having $s < s_{\mathrm{break}}$ continually sprays from colliding bodies having $s > s_{\mathrm{break}}$. We assume that the initial or "injection" spectrum of fresh debris follows a power law; the rate at which grains having sizes between s and $s + ds$ are injected into the entire disk obeys

$$\left. \frac{d\dot{\mathcal{N}}}{ds} \right|_I = C s^{-q_{\mathrm{inject}}}, \qquad (19)$$

where C is a constant and the subscript "I" denotes "injection." Theoretical considerations of mass conservation suggest $q_{\mathrm{inject}} = 3$–4 (Greenberg et al. 1978), while impact experiments using centimeter-sized targets suggest values of $q_{\mathrm{inject}} \approx 3.5$–4 (Fujiwara et al. 1989; see their Fig. 3).

To solve for the steady-state size distribution, we equate the injection rate $d\dot{\mathcal{N}}/ds|_I$ to the removal rate $d\dot{\mathcal{N}}/ds|_R$. We show in § 3.1.3 that removal is dominated by CPR drag onto the central star: $t_{\mathrm{CPR}}/t_{\mathrm{col}} < 1$ for $s < s_{\mathrm{break}}$. Then grains having $s < s_{\mathrm{break}}$ drag inward from the birth ring largely unimpeded by collisions, and

$$\left. \frac{d\dot{\mathcal{N}}}{ds} \right|_R = \frac{1}{t_{\mathrm{CPR}}(s)} \frac{d\mathcal{N}}{ds}. \qquad (20)$$

Equating the injection and removal rates yields

$$\frac{d\mathcal{N}}{ds} \sim C s^{-q_{\mathrm{inject}}} t_{\mathrm{CPR}}(s, \, r_{\mathrm{peri}} = r_{\mathrm{BR}}), \quad s < s_{\mathrm{break}}. \qquad (21)$$
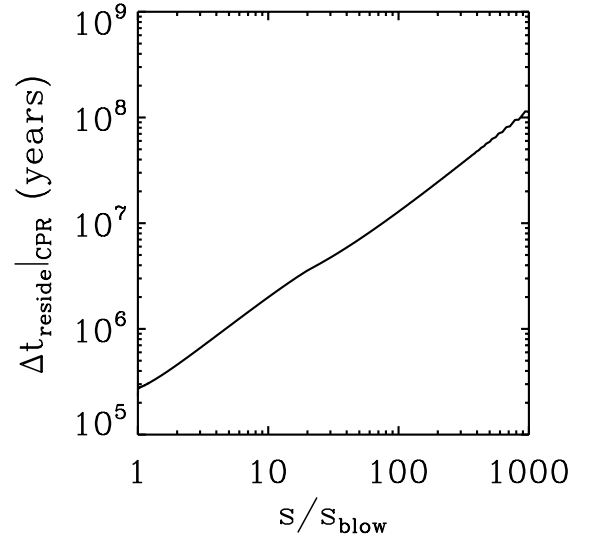

FIG. 2.—Length of time $\Delta t_{\mathrm{reside}}|_{\mathrm{CPR}}$ a grain spends within the birth ring (at radii between $r_{\mathrm{BR}} - \Delta r/2$ and $r_{\mathrm{BR}} + \Delta r/2$) as a function of grain size, for grains whose lifetimes are limited by CPR drag. We take $r_{\mathrm{peri,0}} = r_{\mathrm{BR}} = 43$ AU, $\Delta r/r_{\mathrm{BR}} = 0.1$, and $\dot{M}_* = 1 \dot{M}_\odot$.

The column density dN/ds local to the birth ring is proportional to $d\mathcal{N}/ds$ times the fraction of time spent inside the birth ring:

$$\left. \frac{dN}{ds} \right|_{\mathrm{BR}} \propto \frac{d\mathcal{N}}{ds} \frac{\Delta t_{\mathrm{reside}}|_{\mathrm{CPR}}}{t_{\mathrm{CPR}}} \qquad (22)$$

$$\propto s^{-q_{\mathrm{inject}}} \Delta t_{\mathrm{reside}}|_{\mathrm{CPR}}, \quad s < s_{\mathrm{break}}, \qquad (23)$$

where $\Delta t_{\mathrm{reside}}|_{\mathrm{CPR}}$ is the total time a grain spends inside the birth ring over its CPR-limited lifetime. Figure 2 plots $\Delta t_{\mathrm{reside}}|_{\mathrm{CPR}}$ as a function of s for the parameters $\dot{M}_*/\dot{M}_\odot = 1$, $\Delta r/r_{\mathrm{BR}} = 0.1$, and $r_{\mathrm{peri,0}} = r_{\mathrm{BR}}$. We compute this quantity by explicitly tracking the position of a grain on a decaying orbit. Evidently, $\Delta t_{\mathrm{reside}}|_{\mathrm{CPR}}$ scales approximately linearly with s for all s. We can understand this linear scaling by examining two extremes. For $s \gg s_{\mathrm{blow}}$, orbits are nearly circular always, and $\Delta t_{\mathrm{reside}}|_{\mathrm{CPR}}$ is merely the time for the grain's orbital radius to decay by $\Delta r/2$. This time is proportional to s since $E \approx 1$ (see eq. [12]). For $s - s_{\mathrm{blow}} \ll s_{\mathrm{blow}}$, eccentricities e_0 are large. Over most of a grain's lifetime, the grain's periastron lies inside the birth ring while its apastron lies well outside the birth ring. Evaluated over intervals shorter than t_{CPR}, the fraction of time the grain spends inside the birth ring is given by $f(e)$ with r_{peri} set equal to r_{BR}. Applying equations (11) and (15), we have

$$\Delta t_{\mathrm{reside}}|_{\mathrm{CPR}} \sim \int_{e_0}^0 f(e) \frac{dt}{de} \, de$$

$$\propto s \left(\frac{\Delta r}{r_{\mathrm{BR}}} \right)^{1/2} \int_0^{e_0} \left(\frac{1 + e_0}{1 + e} \right)^2 \left(\frac{e}{e_0} \right)^{3/5} \frac{de}{e_0} \propto s, \quad (24)$$

where the integral in the second row is nearly constant with s.

3.1.2. Equilibrium Size Distribution for $s > s_{\mathrm{break}}$

For $s > s_{\mathrm{break}}$, a collisional cascade is established before CPR drag has time to remove grains. Collisions occur primarily in the

birth ring since the vertical optical depth is greatest there. In the birth ring, the usual collisional equilibrium implies

$$\frac{dN}{ds}\bigg|_{\mathrm{BR}} \propto s^{-q_{\mathrm{ce}}} = s^{-7/2}, \quad s > s_{\mathrm{break}}. \quad (25)$$

By the same logic that led to equation (22),

$$\frac{d\mathcal{N}}{ds} \propto \frac{dN}{ds}\bigg|_{\mathrm{BR}} \frac{t_{\mathrm{col}}}{\Delta t_{\mathrm{reside}}|_{\mathrm{col}}}, \quad s > s_{\mathrm{break}}, \quad (26)$$

where we have assumed (and show in § 3.1.3) that $t_{\mathrm{col}} < t_{\mathrm{CPR}}$ is the appropriate lifetime for grains having $s > s_{\mathrm{break}}$. By analogy to $\Delta t_{\mathrm{reside}}|_{\mathrm{CPR}}$, $\Delta t_{\mathrm{reside}}|_{\mathrm{col}}$ is the total time a grain spends within the birth ring over a collision-limited lifetime.

In the special case of large initial eccentricity e_0,

$$\frac{d\mathcal{N}}{ds} \propto \frac{dN}{ds}\bigg|_{\mathrm{BR}} \frac{1}{f(e_0)}$$
$$\propto \frac{dN}{ds}\bigg|_{\mathrm{BR}} (1 - e_0)^{-3/2}, \quad s > s_{\mathrm{break}}, \; e_0 \approx 1, \quad (27)$$

where we have used the fact that grains having large e_0 and whose lifetimes are limited by $t_{\mathrm{col}} < t_{\mathrm{CPR}}$ have their periastra within the birth ring and their eccentricities close to their birth values for nearly all of their lives.

3.1.3. Optical Depth and Collision Times in the Birth Ring

We estimate the sizes of grains that carry the lion's share of the optical depth in the birth ring. For $s > s_{\mathrm{break}}$, the column density in the birth ring obeys $dN/ds \propto s^{-7/2}$. The vertical optical depth contributed by such grains equals

$$\tau_\perp(s > s_{\mathrm{break}}) \sim s^3 \frac{dN}{ds} \propto s^{-1/2}. \quad (28)$$

Therefore, among grains of size $s > s_{\mathrm{break}}$, the optical depth is dominated by grains of size s_{break}. What about the regime $s < s_{\mathrm{break}}$? From equation (23),

$$\tau_\perp(s < s_{\mathrm{break}}) \sim s^3 \frac{dN}{ds} \propto s^{3-q_{\mathrm{inject}}} \Delta t_{\mathrm{reside}}|_{\mathrm{CPR}}. \quad (29)$$

For $q_{\mathrm{inject}} \approx 3.5\text{--}4$, this quantity either grows or is approximately constant with s. We conclude that grains of size $s \sim s_{\mathrm{break}}$ dominate the total geometric optical depth in the birth ring:

$$\tau_\perp(s_{\mathrm{break}}) \sim \tau_{\perp,\mathrm{BR}}, \quad (30)$$

which in combination with equations (2), (3), and (10) implies that

$$t_{\mathrm{col}}(s_{\mathrm{break}}) \sim t_{c,\mathrm{BR}} (1 - e_{0,\mathrm{break}})^{-3/2}, \quad (31)$$

where $e_{0,\mathrm{break}} \equiv e_0(s_{\mathrm{break}})$.

We exploit equations (2), (10), and (28)–(31) to estimate t_{col} for arbitrary s. For $s > s_{\mathrm{break}}$,

$$t_{\mathrm{col}}(s > s_{\mathrm{break}}) \sim t_{c,\mathrm{BR}} \left(\frac{s}{s_{\mathrm{break}}}\right)^{1/2} (1 - e_0)^{-3/2}, \quad (32)$$

where we have set $e = e_0$ since most of the grain's lifetime is spent with that eccentricity (see § 2.4). Since in the large-s limit $t_{\mathrm{col}} \propto s^{1/2}$ while $t_{\mathrm{CPR}} \propto s$, the assumption made in § 3.1.2 that grains are removed principally by collisions for $s > s_{\mathrm{break}}$ is asymptotically valid. In Figure 1 we plot equation (32) as a fiducial

size-dependent collision time, replacing s_{break} by s_{blow} to render the curve independent of stellar mass-loss rate. This replacement, performed solely for Figure 1, accrues only a slight error since we find in § 3.1.4 that s_{break} and s_{blow} are nearly the same.

Next we estimate $t_{\mathrm{col}}(s < s_{\mathrm{break}})$ and show that $t_{\mathrm{CPR}}/t_{\mathrm{col}} < 1$ for $s < s_{\mathrm{break}}$, as was assumed in § 3.1.1. Equation (30) implies that grains having $s < s_{\mathrm{break}}$ are predominantly destroyed by s_{break}-sized grains. Then[7]

$$t_{\mathrm{col}}(s < s_{\mathrm{break}}) \sim \frac{1}{\Omega(s)\tau_\perp(s_{\mathrm{break}})}$$
$$\sim t_{\mathrm{col}}(s_{\mathrm{break}}) \left(\frac{1 - e_{0,\mathrm{break}}}{1 - e_0}\right)^{3/2}. \quad (33)$$

For convenience, we construct the approximate fitting formula for t_{CPR} from equations (12), (16), and (17):

$$t_{\mathrm{CPR}}(s < s_{\mathrm{break}}) \sim t_{\mathrm{col}}(s_{\mathrm{break}}) \left(\frac{s}{s_{\mathrm{break}}}\right) \left(\frac{1 - e_{0,\mathrm{break}}}{1 - e_0}\right)^{1/2}. \quad (34)$$

Combining equations (33) and (34), we find that the ratio between CPR and collision lifetimes is

$$\frac{t_{\mathrm{CPR}}}{t_{\mathrm{col}}}\bigg|_{s < s_{\mathrm{break}}} \sim \left(\frac{s}{s_{\mathrm{break}}}\right) \left(\frac{1 - e_0}{1 - e_{0,\mathrm{break}}}\right) < 1. \quad (35)$$

Indeed, this ratio vanishes as s approaches s_{blow}. We have established that the inequality given by equation (35) holds at $r = r_{\mathrm{BR}}$, but in fact it holds for all $r = r_{\mathrm{peri}} < r_{\mathrm{BR}}$, since $t_{\mathrm{CPR}} \propto r^2$ while $t_{\mathrm{col}} \propto r^{3/2}$. Therefore, our assumption that bound grains having $s < s_{\mathrm{break}}$ are removed principally by CPR drag is valid.

3.1.4. Calculating s_{break}

Equate the collision time (eq. [32]) to the CPR drag time (eq. [12]),

$$(1 - e_{0,\mathrm{break}})^{-3/2} t_{c,\mathrm{BR}} \sim \frac{4\pi c^2 \rho r_{\mathrm{BR}}^2}{3L_* P_{\mathrm{CPR}}} s_{\mathrm{break}} E(e_{0,\mathrm{break}}), \quad (36)$$

to find

$$s_{\mathrm{break}} \sim \begin{cases} 1.002 s_{\mathrm{blow}} = 0.2 \; \mu\mathrm{m}, & \dot{M}_*/\dot{M}_\odot = 1, \\ 1.01 s_{\mathrm{blow}} = 0.2 \; \mu\mathrm{m}, & \dot{M}_*/\dot{M}_\odot = 10, \\ 1.1 s_{\mathrm{blow}} = 0.3 \; \mu\mathrm{m}, & \dot{M}_*/\dot{M}_\odot = 10^2, \\ 2.3 s_{\mathrm{blow}} = 2 \; \mu\mathrm{m}, & \dot{M}_*/\dot{M}_\odot = 10^3. \end{cases} \quad (37)$$

3.1.5. Larger Parent Bodies

Bodies having $s > s_{\mathrm{break}}$ participate in a collisional cascade in which the Dohnanyi-like spectrum extends from s_{break} up to a maximum size s_{max}. By definition, s_{max} characterizes those grains whose collisional lifetimes equal the age of the AU Mic disk; by equation (32), this size satisfies

$$t_{\mathrm{col}}(s_{\mathrm{max}}) \sim t_{c,\mathrm{BR}} \left(\frac{s_{\mathrm{max}}}{s_{\mathrm{break}}}\right)^{1/2} = t_{\mathrm{age}}, \quad (38)$$

---

[7] Equation (33) overestimates t_{col} because it neglects the fact that grains on highly eccentric orbits intercept an optical depth parallel to the disk in addition to $\tau_{\perp,\mathrm{BR}}$. This neglect does not change our derived scaling relations, but it will change certain normalizations, e.g., the threshold $\dot{M}_*$ dividing CPR-dominated from collision-dominated behavior. We are indebted to Y. Wu for pointing out this omission, which will need to be corrected in future work.

where we have dropped the eccentricity-dependent factor since grains having $s = s_{\max} \gg s_{\mathrm{blow}}$ travel on essentially circular orbits. Then

$$s_{\max} \sim \left(\frac{t_{\mathrm{age}}}{t_{c,\mathrm{BR}}}\right)^2 s_{\mathrm{break}} \sim \begin{cases} 10 \text{ cm}, & \dot{M}_*/\dot{M}_\odot = 1, \\ 10 \text{ cm}, & \dot{M}_*/\dot{M}_\odot = 10, \\ 20 \text{ cm}, & \dot{M}_*/\dot{M}_\odot = 10^2, \\ 100 \text{ cm}, & \dot{M}_*/\dot{M}_\odot = 10^3. \end{cases} \quad (39)$$

Our model has no information on parent bodies having $s > s_{\max}$. While such bodies likely exist, we do not know whether they are currently in a constructive (planet building) or destructive (debris generating) phase of their evolution. It is not justified to extend the size distribution to $s > s_{\max}$ (e.g., to the kilometer size range) as is sometimes done.

3.2. Physical Implications of Optical Depth Profiles

The birth ring divides the inner disk from the outer disk. In § 3.2.1 we discuss the vertical optical depth in the inner disk. In § 3.2.2 we estimate the total disk mass. In § 3.2.3 we derive analytically how the vertical optical depth scales with radius in the outer disk.

3.2.1. Inner Disk ($r < r_{\mathrm{BR}}$): Competition between Collisions and CPR-driven Accretion

We showed in § 3.1.3 that grains of size $s \sim s_{\mathrm{break}}$ make the largest contribution to the total optical depth at $r \approx r_{\mathrm{BR}}$. Bound grains having $s < s_{\mathrm{break}}$ tend to be transported inward by CPR drag, unimpeded by interparticle collisions. Larger grains tend to be collisionally destroyed before reaching the star. How does the vertical optical depth in the inner disk compare with the optical depth in the birth ring?

We define CPR-dominated type A disks to be systems for which $s_{\mathrm{break}} - s_{\mathrm{blow}} \gg s_{\mathrm{blow}}$. In such disks, grains for which $s_{\mathrm{blow}} < s < s_{\mathrm{break}}$ are numerous, contain a significant fraction of the total optical depth in the birth ring, and tend to accrete onto the central star before undergoing a collision. From continuity, the optical depth $\tau_\perp(r < r_{\mathrm{BR}})$ scales approximately as r^0: the inner disk is "filled in."

By contrast, in collision-dominated type B disks, $s_{\mathrm{break}} - s_{\mathrm{blow}} \ll s_{\mathrm{blow}}$. The region inside the birth ring is virtually empty. The reasons for this are twofold. First, the range of sizes of grains that drag in without being collisionally destroyed ($s_{\mathrm{blow}} < s < s_{\mathrm{break}}$) is narrow; there are not many such grains. Second, because s_{break} is so close to s_{blow}, s_{break}-sized grains have large initial eccentricity. They spend most of their lifetimes having $r_{\mathrm{peri}} \approx r_{\mathrm{peri},0}$ and only a small portion at $r < r_{\mathrm{BR}}$ (see § 2.4).

As judged from equation (37), if $\dot{M}_*/\dot{M}_\odot \gg 10^2$, type A conditions would hold for the AU Mic disk and the inner disk would be filled in. If $\dot{M}_*/\dot{M}_\odot \ll 10^2$, then type B conditions would hold and the inner disk would be empty. In § 4 we not only check these assertions by detailed Monte Carlo simulations of the AU Mic disk but also decide which case is favored by the observations.

3.2.2. Total Mass of the Disk

By equation (25), most of the mass of the disk is contributed by the largest grains ($s = s_{\max}$), since $s^4 \, dN/ds \propto s^{1/2}$. We scale from the column density of s_{break}-sized grains in the birth ring,

$$\tau_{\perp,\mathrm{BR}} \sim \pi s_{\mathrm{break}}^3 \left.\frac{dN}{ds}\right|_{s_{\mathrm{break}}}, \quad (40)$$

to estimate the column density of $s_{\max}$-sized grains in the birth ring,

$$s_{\max} \left.\frac{dN}{ds}\right|_{s_{\max}} \sim \frac{\tau_{\perp,\mathrm{BR}}}{\pi s_{\mathrm{break}}^3} \left(\frac{s_{\max}}{s_{\mathrm{break}}}\right)^{-7/2} s_{\max}. \quad (41)$$

The total number of such grains is their column density multiplied by the area of the birth ring $2\pi r_{\mathrm{BR}} \Delta r$, since $s_{\max}$-sized grains undergo a collision long before dragging inward. Multiplying this total number by the mass of a single grain yields the mass of the disk,

$$M_{\max} \sim \frac{8\pi}{3} \rho r_{\mathrm{BR}} \tau_{\perp,\mathrm{BR}} s_{\mathrm{break}} \left(\frac{s_{\max}}{s_{\mathrm{break}}}\right)^{1/2} \Delta r$$

$$\sim 0.01 \, M_\oplus \left(\frac{\Delta r/r_{\mathrm{BR}}}{0.1}\right) \left(\frac{\tau_{\perp,\mathrm{BR}}}{4 \times 10^{-3}}\right)^2 \left(\frac{s_{\mathrm{break}}}{0.2 \, \mu\mathrm{m}}\right), \quad (42)$$

where we have used equations (2) and (39) and have normalized $\Delta r/r_{\mathrm{BR}}$ and $\tau_{\perp,\mathrm{BR}}$ to values that yield good fits to observations, as described in § 4. The steady comminution of $\sim 0.01 \, M_\oplus \sim 1$ lunar mass's worth of decimeter-sized bodies into micron-sized particles does not seem an unduly heavy burden for the AU Mic system to bear. The solar system is thought to have somehow shed $\sim 10 \, M_\oplus$ of rock and ice near ~ 30 AU over an uncertain timescale of 10–1000 Myr during its "cleanup" phase (Goldreich et al. 2004).

3.2.3. Outer Disk ($r > r_{\mathrm{BR}}$): Barely Bound Grains

Grains created at $r = r_{\mathrm{BR}} = 43$ AU and having $s - s_{\mathrm{blow}} \lesssim s_{\mathrm{blow}}$ occupy initially highly eccentric orbits having periastron distances $r_{\mathrm{peri}} = r_{\mathrm{BR}}$ (see § 2.3). Here we show that such barely bound grains establish an outer disk at $r \gg r_{\mathrm{BR}}$ whose vertical optical depth scales approximately as $r^{-5/2}$ for CPR-dominated type A disks and as $r^{-3/2}$ for collision-dominated type B disks. The contribution of unbound grains having $s \leq s_{\mathrm{blow}}$ relative to that of barely bound grains is assessed in § 3.3.

The outer disk comprises grains having sizes slightly greater than s_{blow} since only those grains have substantial eccentricities (see eqs. [9a]–[9c]). We refer to such barely bound grains as having sizes $s = s_{\mathrm{blow},+}$. The optical depth in the outer disk should scale approximately as their column density $N_{\mathrm{blow},+}$:

$$\tau_\perp \propto N_{\mathrm{blow},+} \propto \frac{1}{r} \frac{d\mathcal{N}_{\mathrm{blow},+}}{dr}, \quad (43)$$

where $\mathcal{N}_{\mathrm{blow},+}$ is the total number of such grains in the entire disk (see eq. [18]). By the chain rule,

$$\frac{d\mathcal{N}_{\mathrm{blow},+}}{dr} = \frac{d\mathcal{N}_{\mathrm{blow},+}}{de} \frac{de}{dr}. \quad (44)$$

We determine de/dr by making the approximation that at any instant, all grains are located at their apastra:

$$e = \frac{r_{\mathrm{apo}} - r_{\mathrm{peri}}}{r_{\mathrm{apo}} + r_{\mathrm{peri}}} \quad (45)$$

$$\approx \frac{r - r_{\mathrm{BR}}}{r + r_{\mathrm{BR}}}. \quad (46)$$

This approximation should be good for the highly eccentric orbits of the outer disk. Differentiating equation (46), we find for $r \gg r_{BR}$ that

$$\frac{de}{dr} \approx \frac{2r_{BR}}{(r + r_{BR})^2} \propto \frac{1}{r^2}. \tag{47}$$

The remaining factor in equation (44), $d\mathcal{N}_{blow,+}/de$, is determined by the size distribution of barely bound grains. This differs between type A and type B disks, as seen below. The size distribution determines the initial shape of the eccentricity distribution. The eccentricity distribution is altered over time by CPR drag. Consider grains having identical initial eccentricities e_0 created at a constant rate $\tilde{\mathcal{N}}$. In steady state, CPR drag transports a constant number of particles per time through eccentricity space, $(d\tilde{\mathcal{N}}/de)(de/dt) \sim \tilde{\mathcal{N}}$. Hence,

$$\frac{d\tilde{\mathcal{N}}}{de} \propto \left(\frac{de}{dt}\right)^{-1} \propto \frac{e^{3/5}}{(1 - e^2)^{3/2}}, \quad e \leq e_0, \tag{48}$$

where we have used equation (15). Equation (48) implies that nearly all barely bound grains have $e \approx e_0$. Therefore, the CPR-evolved eccentricity distribution closely resembles the initial eccentricity distribution:

$$\frac{d\mathcal{N}}{de} \sim \frac{d\mathcal{N}}{de_0}. \tag{49}$$

Now we address the size distribution that determines $d\mathcal{N}/de_0$. For type A disks, for which $s_{break} - s_{blow} \gg s_{blow}$, the size distribution for barely bound grains obeys $d\mathcal{N}/ds \propto s^{-q_{inject}} t_{CPR}(s)$ (see eq. [21]). For type B disks, $s_{break} - s_{blow} \ll s_{blow}$; outer-disk grains for which $s_{blow} < s < s_{break}$ are outnumbered by grains having $s > s_{break}$. The relevant size distribution in the outer regions of type B disks is therefore the one appropriate for $s > s_{break}$: $d\mathcal{N}/ds \propto s^{-7/2}(1 - e_0)^{-3/2}$ (see eq. [27]).[8] We evaluate these distributions for $s = s_{blow,+}$:

$$\frac{d\mathcal{N}_{blow,+}}{ds} \propto E(e_0) \propto (1 - e_0)^{-1/2} \tag{50a}$$

and

$$\frac{d\mathcal{N}_{blow,+}}{ds} \propto (1 - e_0)^{-3/2} \tag{50b}$$

for type A and type B disks, respectively, using equations (12) and (16). Now $d\mathcal{N}/de \sim d\mathcal{N}/de_0 = (d\mathcal{N}/ds)(ds/de_0)$. Since equations (9a)–(9c) imply that ds/de_0 is approximately constant for $e_0 \approx 1$ (i.e., for $s = s_{blow,+}$), and since $r \approx r_{apo} \approx 2r_{BR}/(1 - e_0)$,

$$\frac{d\mathcal{N}_{blow,+}}{de} \propto (1 - e_0)^{-1/2} \propto r^{1/2} \tag{51a}$$

and

$$\frac{d\mathcal{N}_{blow,+}}{de} \propto (1 - e_0)^{-3/2} \propto r^{3/2} \tag{51b}$$

[8] This statement for type B disks is only valid not too far from the birth ring. As $r \to \infty$, the only bound grains that are present have sizes between s_{blow} and s_{break}. These obey $\tau_\perp \propto r^{-5/2}$, just as they do for type A disks. Therefore, for type B disks, the $\tau_\perp \propto r^{-3/2}$ scaling derived in the main text eventually gives way to $\tau_\perp \propto r^{-5/2}$.

for type A and type B disks, respectively. Combine equations (43), (44), (47), (51a), and (51b) to obtain

$$\tau_\perp \propto r^{-5/2} \tag{52a}$$

and

$$\tau_\perp \propto r^{-3/2} \tag{52b}$$

for type A and type B disks, respectively. Note that these scaling relations cannot be obtained by merely assuming that the disk-integrated size distribution obeys the usual Dohnanyi relation $d\mathcal{N}/ds \propto s^{-7/2}$. For type B disks, for example, the key modification arises from the prolonging of the collisional lifetime due to SWR pressure [i.e., the factor of $(1 - e_0)^{-3/2}$ in eq. (51b)]. Moreover, the scalings are robust against uncertainties in the size distribution; they do not depend explicitly on either q_{ce} or q_{inject}. We verify these scalings by numerical experiments in § 4.

3.3. Unbound Grains ($\beta \geq \frac{1}{2}$)

The rapid expulsion of unbound ($\beta \geq \frac{1}{2}$) grains compared to the longer, CPR-driven orbital decay of barely bound ($\frac{1}{2} - \beta \ll 1$) grains suggests that in steady state, unbound grains contribute little to the surface brightness of the outer disk. On the other hand, unbound grain velocities are nearly constant with radius: for $\beta \approx 1$, velocities are approximately equal to their (circular, Keplerian) birth velocities. As a result, the optical depth of unbound grains should roughly obey $\tau_{\perp,ub} \propto r^{-1}$ and should eventually exceed, at some "crossover radius," the optical depth of barely bound grains, which scales as $\tau_{\perp,bb} \propto r^{-5/2}$ in type A disks and as $\tau_{\perp,bb} \propto r^{-3/2}$ in type B disks (§ 3.2.3). In this section we estimate the value of the crossover radius, r_{cross}, and show in the case of AU Mic that it lies outside the scope of current observations.

Consider a type A disk. In the birth ring, the optical depth of barely bound grains exceeds that of unbound grains by

$$\frac{\tau_{\perp,bb}}{\tau_{\perp,ub}} \sim \frac{\int_{s_{blow}}^{2s_{blow}} (dN/ds)s^2 \, ds}{\int_{\min(s_V)}^{s_{blow}} (dN/ds)s^2 \, ds}. \tag{53}$$

The smallest unbound grain of interest is the smallest grain for which $Q_{scat} \sim 1$: $\min(s_V) \approx 0.1 \; \mu$m. Since $\tau_{\perp,bb} \propto r^{-5/2}$ while $\tau_{\perp,ub} \propto r^{-1}$, the crossover radius is

$$r_{cross} \sim \left(\frac{\tau_{\perp,bb}}{\tau_{\perp,ub}}\right)^{2/3} r_{BR}. \tag{54}$$

By equation (23),

$$\left. \frac{dN}{ds} \right|_{s_{blow} < s < 2s_{blow}} \sim Ds^{-q_{inject}} \Delta t_{reside} |_{CPR} \tag{55}$$

in the birth ring, where D is a constant. By the same logic that led to equation (23),

$$\left. \frac{dN}{ds} \right|_{s < s_{blow}} \sim Ds^{-q_{inject}} t_{blow}(s) \tag{56}$$

in the birth ring, where

$$t_{blow}(s) \sim \frac{\sqrt{r_{BR}\Delta r}}{\Omega_{BR} r_{BR} \sqrt{\beta}} \sim 90 \left(\frac{s}{s_{blow}}\right)^{1/2} \sqrt{\frac{\Delta r}{r_{BR}}} \; \text{yr} \tag{57}$$

is the time for an unbound grain to leave the birth ring, and $\Omega_{BR} = (GM_*/r_{BR}^3)^{1/2}$. Numerical evaluation of the integrals in equation (53) reveals that

$$r_{cross} \sim \begin{cases} 900 \text{ AU}, & \dot{M}_*/\dot{M}_\odot = 10^2, \\ 200 \text{ AU}, & \dot{M}_*/\dot{M}_\odot = 10^3. \end{cases} \quad (58)$$

If instead type B conditions apply for the AU Mic disk, then by considerations analogous to those above, $r_{cross} \gg 10^3$ AU. We compare r_{cross} with the maximum radius probed by current observations, approximately 200 AU, to conclude that under type A conditions, unbound grains contribute at most marginally to the currently observed surface brightness. Under type B conditions, they contribute negligibly.

3.4. *Unequilibrated Grains* ($s_{blow} < s < s_{age}$)

Grains on extremely eccentric orbits may have collisional and CPR lifetimes that exceed the age of the system. Can such grains, whose numbers cannot be assessed within our steady-state model, contribute significantly to the observed surface brightness of the AU Mic disk? Such "unequilibrated grains" have sizes between s_{blow} and s_{age}, where

$$t_{age} = \min\left[t_{CPR}(s_{age}), \ t_{col}(s_{age})\right] \quad (59)$$

defines s_{age}. We apply equations (12) and (33) to find that

$$\frac{s_{age}}{s_{blow}} \sim \begin{cases} 1.006, & \dot{M}_*/\dot{M}_\odot = 1, \\ 1.002, & \dot{M}_*/\dot{M}_\odot = 10, \\ 1.00003, & \dot{M}_*/\dot{M}_\odot = 10^2, \\ 1.000002, & \dot{M}_*/\dot{M}_\odot = 10^3. \end{cases} \quad (60)$$

Unequilibrated grains occupy such a narrow range of sizes that they seem unlikely to contribute much to the total optical depth. We ignore the unequilibrated population for the remainder of this paper.

4. MONTE CARLO MODELING

4.1. *Procedure*

To test several of the analytic results derived in § 3, we model the AU Mic disk by means of a Monte Carlo simulation. We calculate the geometric optical depth $\tau_\perp(r)$, edge-on surface brightness profile SB(b), and spectral flux density F_ν, and then we compare to observations. The input parameters are the stellar mass-loss rate $\dot{M}_*$, optical depth in the center of the birth ring $\tau_{\perp, BR} \equiv \tau_\perp(r_{BR})$, and width of the birth ring Δr.

We lay down a number J of dust particles around the central star in a two-dimensional plane. Each particle's radial coordinate r and azimuth ψ are determined by the particle's semimajor axis a, eccentricity e, true anomaly ϕ_t, and longitude of periastron $\tilde{\omega}$. Since our model disk is axisymmetric, $\tilde{\omega}$ is drawn as a uniform deviate from 0 to 2π.

The birth distributions of the remaining orbital elements depend on the distribution of grain sizes s. Orbital elements subsequently evolve from their birth values by CPR drag. The degree of evolution depends on the age of the grain (t) relative to the CPR lifetime (t_{CPR}; eq. [12]) and the collision lifetime (t_{col}; eqs. [32] and [33]). By definition, s_{break} is the grain size for which $t_{CPR} = t_{col}$, and s_{age} is the smallest grain size for which $\min(t_{CPR}, \ t_{col}) = t_{age}$. Only grains having $s > s_{age}$ can be removed over the age of the system. For $s > s_{break}$, collisions are more important than

CPR drag in removing grains ($t_{col} < t_{CPR}$), so we draw the ages t of such particles as a uniform deviate from 0 to $t_{col}(s)$. Grains of size $s < s_{break}$ are removed by CPR drag ($t_{CPR} < t_{col}$), so we draw t for these grains as a uniform deviate from 0 to $t_{CPR}(s)$.

The evolved eccentricity e depends on the initial eccentricity e_0 and the age of the particle, implicitly according to

$$\frac{t}{t_{CPR}} = 1 - \frac{E(e)}{E(e_0)} \left(\frac{1+e_0}{1+e}\right)^2 \left(\frac{e}{e_0}\right)^{8/5}, \quad (61)$$

where $E(e)$ is defined by equation (14). The evolved semimajor axis is given by

$$a = a_0 \left(\frac{e}{e_0}\right)^{4/5} \left(\frac{1-e_0^2}{1-e^2}\right) \quad (62)$$

(Wyatt & Whipple 1950), where the initial semimajor axis a_0 is derived from the initial periastron $r_{peri,0}$, which we draw in the following way. In our model, all grains are born in the birth ring, an annulus of width Δr centered at r_{BR}. At birth, a grain is located at the periastron of its osculating orbit—an orbit rendered eccentric by SWR forces (§ 2.3). We draw $r_{peri,0}$ from a uniform distribution of width Δr centered at r_{BR}.

As mentioned, the birth distributions of eccentricities and semimajor axes depend on the distribution of grain sizes s. Although particles in our simulation are born only in the birth ring, their steady-state population may occupy all space, so we must draw s from the global, disk-integrated size distribution $d\mathcal{N}/ds$. We apply results from § 3.1, made more precise for our Monte Carlo calculation. From equation (21),

$$\frac{d\mathcal{N}}{ds} \propto s^{-q_{inject}} t_{CPR}(s, \ r_{peri} = r_{BR}), \quad s_{age} < s < s_{break}, \quad (63)$$

and from equation (26),

$$\frac{d\mathcal{N}}{ds} \propto s^{-7/2} \frac{t_{col}}{\Delta t_{reside}|_{col}}, \quad s > s_{break}. \quad (64)$$

We approximate t_{col} using equation (32), and we evaluate $\Delta t_{reside}|_{col}$ numerically. We take the distribution described by equations (63) and (64) to be nonzero only for $s > s_{age}$[9] and to be continuous across s_{break}; furthermore, we truncate the distribution at $s_{max} = 500 s_{blow}$ because of computational limitations. We fix $q_{inject} = 4$. The distribution $d\mathcal{N}/ds$ is plotted in Figure 3. For each s drawn, e_0 and a_0 are calculated using equations (9a)–(9c). For $J = 10^9$, one Monte Carlo simulation takes 8 hr to complete on a 1.33 GHz PowerPC G4 processor.

That the distribution of mean anomalies ϕ_m is uniform determines the distribution of true anomalies ϕ_t via Kepler's equation (Murray & Dermott 1999):

$$\phi_m = \phi_e - e \sin \phi_e, \quad (65)$$

where ϕ_e is the eccentric anomaly:

$$\tan \frac{\phi_t}{2} = \left(\frac{1+e}{1-e}\right)^{1/2} \tan \frac{\phi_e}{2}. \quad (66)$$

---

[9] For $\dot{M}_*/\dot{M}_\odot = 1$, $s_{age} > s_{break}$ so only eq. (64) is relevant.

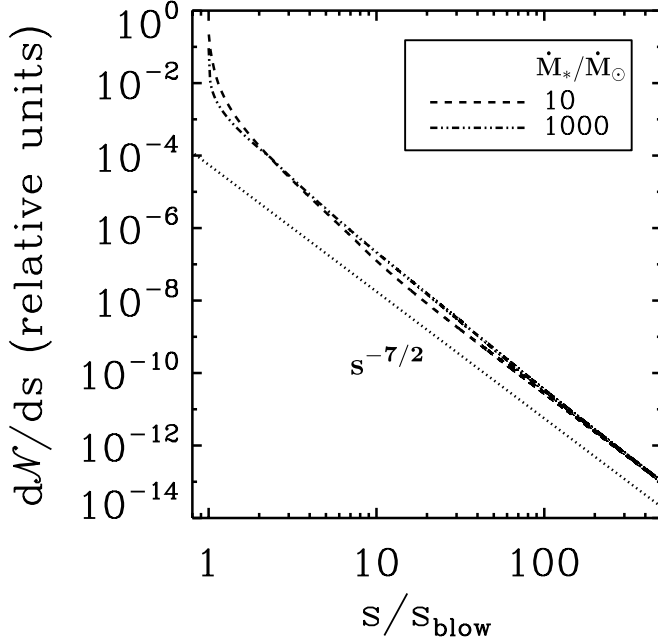FIG. 3.—Disk-integrated grain size distributions $d\mathcal{N}/ds$. Dashed and double-dot–dashed curves correspond, respectively, to $\dot{M}_*/\dot{M}_\odot = \{10,\ 10^3\}$. A dotted line proportional to the Dohnanyi scaling $s^{-q_{cc}} = s^{-7/2}$ is overplotted for reference. As s approaches s_{blow}, the population of grains rises significantly above what one would expect from a pure Dohnanyi size spectrum. The deviations from a Dohnanyi spectrum, which differ under type A (e.g., $\dot{M}_* = 10^3 \dot{M}_\odot$) and type B (e.g., $\dot{M}_* = 10 \dot{M}_\odot$) conditions, are critical for understanding how $\tau_\perp$ scales with r in the outer disk; see § 3.2.3.

Knowing a, e, and ϕ_t for each particle determines its radial distance from the star:

$$r = \frac{a(1 - e^2)}{1 + e \cos \phi_t}. \tag{67}$$

4.2. Products of the Monte Carlo Calculation

Having laid down J particles of various sizes, we output the following:

1. The geometric vertical optical depth $\tau_\perp(r)$. We first calculate this quantity in relative units by summing the geometric cross sections of particles in a given annulus and dividing the resultant sum by the area of that annulus. We then normalize this result by matching the input $\tau_{\perp, BR}$ to the model's relative optical depth at r_{BR}.

2. The surface brightness of the disk observed edge-on at V-band (*Hubble Space Telescope*'s F606W) and H-band wavelengths, as a function of projected stellar separation b:

$$\text{SB}(b,\ \lambda)$$
$$= \int \int \frac{\lambda L_{\lambda,*}}{4\pi r^2} Q_{\text{scat}}(\lambda,\ s) P(\theta,\ \lambda,\ s) \pi s^2 \frac{dn}{ds}(r,\ s)\, d\ell\, ds, \tag{68}$$

where $\ell = \pm(r^2 - b^2)^{1/2}$ measures distance along our line of sight. The stellar flux incident on a grain in the wave band of interest is $\lambda L_{\lambda,*}/4\pi r^2$, the cross section for scattering is $Q_{\text{scat}} \pi s^2$, the scattering angle between the star, grain, and observer is $\theta = \tan^{-1}(\ell/b)$, and the relative power scattered per steradian is P (normalized so that its integral over all solid angle equals unity). We use Mie theory to calculate Q_{scat} and P, adopting the optical constants of pure water ice (Warren 1984). The volumetric

number density of grains n is found by dividing the geometric vertical optical depth by the height of the disk:

$$\pi s^2 \frac{dn}{ds}(r,\ s) = \frac{1}{h(r)} \frac{d\tau_\perp}{ds}(r,\ s). \tag{69}$$

The radial height profile $h(r)$ is derived from the projected disk height $h(b)$, which roughly follows a broken power law that changes slope around $b = r_{BR} = 43$ AU:

$$h(b) = h_{BR} \begin{cases} (b/r_{BR})^{\eta_1}, & b < r_{BR}, \\ (b/r_{BR})^{\eta_2}, & b > r_{BR}. \end{cases} \tag{70}$$

We set $h_{BR} = 2.75$ AU. K05 fit separate broken power laws to the northwest and southeast extensions of the disk and obtain $\eta_1 \approx 0$ and $\eta_2 \approx 1$–2 (see their Fig. 7). For simplicity, we take $\eta_1 = 0$ and $\eta_2 = 1$. These values characterize an inner disk that is empty and seen in projection (or that has constant height) and an outer disk in which grains have constant inclination dispersion. We adopt a radial profile $h(r)$ identical to $h(b)$ as given in equation (70) with b replaced by r. We divide the F606W profile by the H profile to obtain a $V - H$ color profile.

3. The spectral flux density F_ν:

$$F_\nu = \frac{1}{d^2} B_\nu(T_*) \pi R_*^2$$
$$+ \frac{1}{d^2} \int \int B_\nu(T(r,\ s)) Q_{\text{emis}}(\lambda,\ s) \pi s^2 \frac{dN}{ds}(r,\ s) 2\pi r\, dr\, ds, \tag{71}$$

where $B_\nu(T)$ is the Planck function. We model the emissivity of the dust as a broken power law:

$$Q_{\text{emis}} = \begin{cases} 1, & 2\pi s > \lambda, \\ 2\pi s/\lambda, & \text{otherwise,} \end{cases} \tag{72}$$
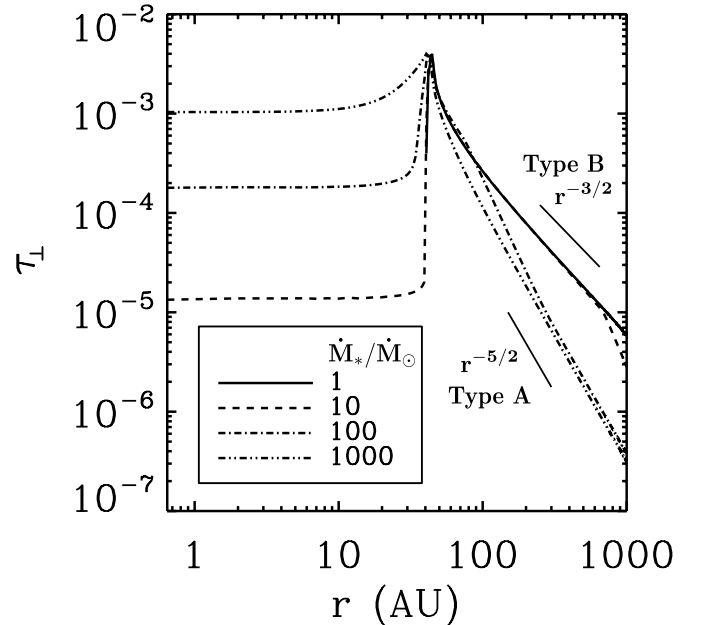

FIG. 4.—Vertical optical depth profiles computed from our Monte Carlo simulations. Solid, dashed, dot-dashed, and double-dot–dashed curves correspond, respectively, to $\dot{M}_*/\dot{M}_\odot = \{1, 10, 10^2, 10^3\}$. Values for $\tau_{\perp, BR} = 0.004$ and $\Delta r/r_{BR} = 0.1$ are held fixed for all models. The two types of disks, CPR-dominated type A disks and collision-dominated type B disks, may be distinguished. The inner disk for $\dot{M}_* = 1 \dot{M}_\odot$ is completely empty because $s_{\text{break}} < s_{\text{age}}$.
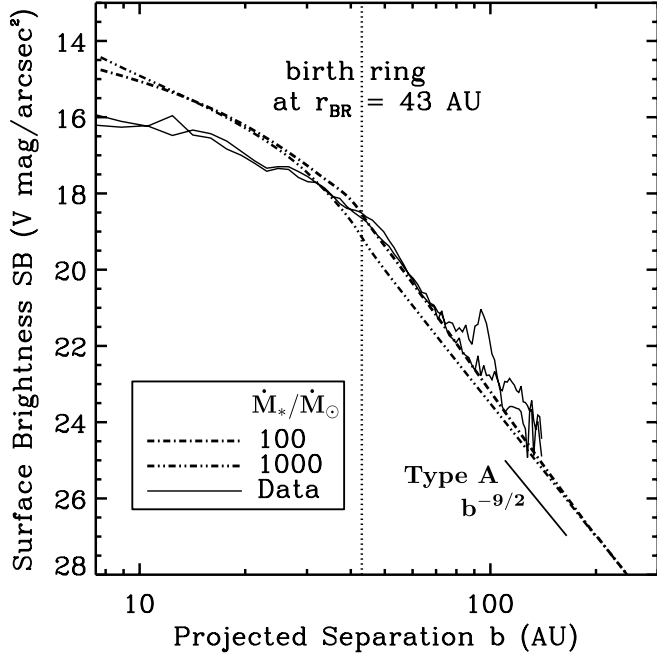
FIG. 5.—Theoretical type A and observed surface brightness profiles. Thin lines are data (for northwest and southeast extensions of the disk) from K05. Dot-dashed and double-dot–dashed curves correspond, respectively, to $\dot{M}_*/\dot{M}_\odot = \{10^2, 10^3\}$. The vertical dotted line corresponds to $r_{BR} = 43$ AU, the radius of the birth ring containing dust-producing parent bodies. The inset scaling of $b^{-9/2}$ is derived from the rule of thumb that at large b, SB $\propto b^{\gamma-\eta-1}$ for $h \propto r^\eta$ and $\tau_\perp \propto r^\gamma$. According to our theory for type A disks, $\eta = 1$ and $\gamma = -5/2$.
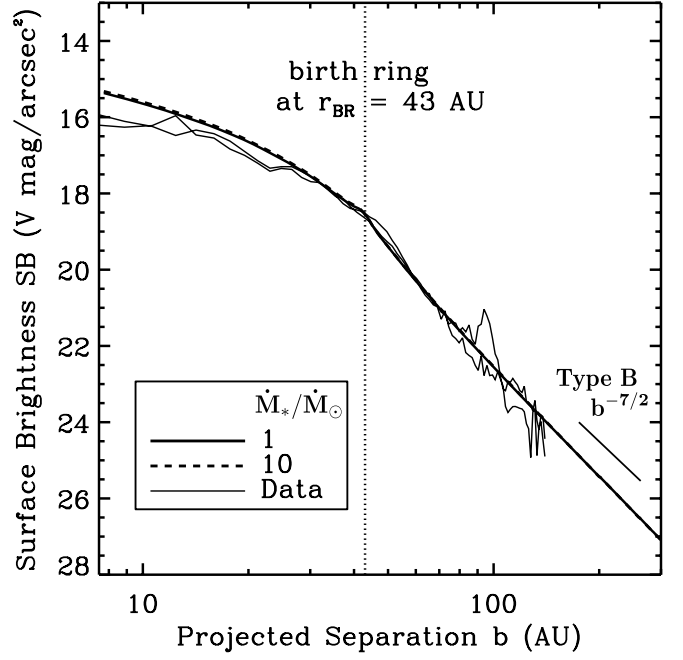

FIG. 6.—Same as Fig. 5, but for type B disk models. Thick solid and dashed curves correspond, respectively, to $\dot{M}_*/\dot{M}_\odot = \{1, 10\}$. The vertical dotted line corresponds to $r_{BR} = 43$ AU, the radius of the birth ring containing dust-producing parent bodies. The inset scaling of $b^{-7/2}$ is derived from the rule of thumb that at large b, SB $\propto b^{\gamma-\eta-1}$ for $h \propto r^\eta$ and $\tau_\perp \propto r^\gamma$. According to our theory for type B disks, $\eta = 1$ and $\gamma = -3/2$. Stellar mass-loss rates of $(1–10)\dot{M}_\odot$ yield surface brightness profiles that agree better with the data than those derived from rates of $(10^2–10^3)\dot{M}_\odot$; contrast with Fig. 5.
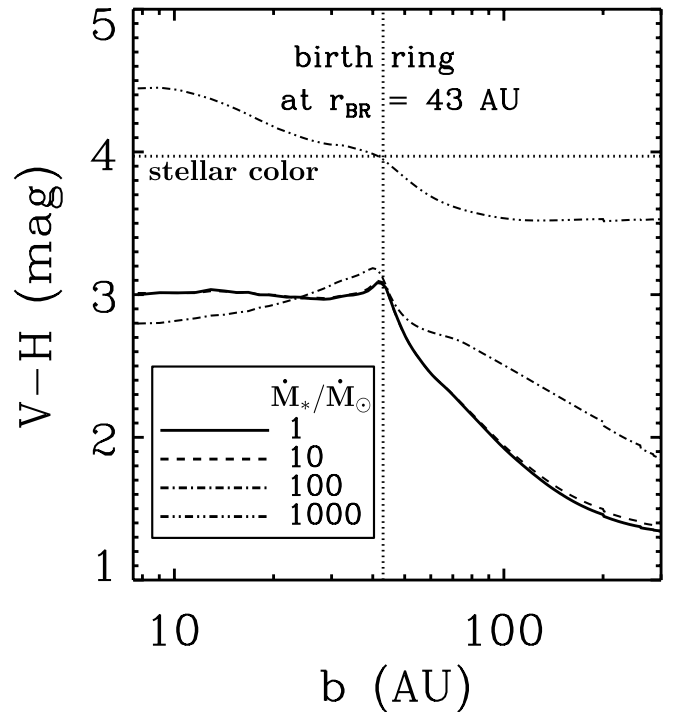
in approximate agreement with the model of Chiang et al. (2001) for ice-mantled silicate grains. Since the peak wavelength of emission from AU Mic is about 1 μm, all bound grains are large enough to absorb most of the incident stellar flux. We solve

$$\frac{L_*}{4\pi r^2}\pi s^2 = 4\pi \int_0^\infty B_\lambda(T)Q_{\rm emis}(\lambda,\ s)\pi s^2\, d\lambda \qquad (73)$$

for the temperature T specific to a given grain size.

4.3. Results

By experimenting with various values of $\tau_{\perp,BR}$, Δr, and $\dot{M}_* \in (1, 10, 10^2, 10^3)\dot{M}_\odot$, we find that $\tau_{\perp,BR} = 4 \times 10^{-3}$, $\Delta r/r_{BR} = 0.1$, and $\dot{M}_* \in (1, 10)\dot{M}_\odot$ yield theoretical surface brightness profiles and spectra that agree encouragingly well with observations. Our preferred values for $\tau_{\perp,BR}$ and Δr are likely uniquely determined to within factors of a few; SB($b = r_{BR}$) $\propto \tau_{\perp,BR}(\Delta r)^{1/2}$ while $F_\nu \propto \tau_{\perp,BR}\Delta r$. The close resemblance of the models for which $\dot{M}_* \lesssim 10\dot{M}_\odot$ means that we cannot do better than place an upper limit on $\dot{M}_*/\dot{M}_\odot$ of $\sim$10. In what follows, we present results for our preferred input parameters, in addition to models for which $\dot{M}_* \in (10^2, 10^3)\dot{M}_\odot$ to study the effect of varying $\dot{M}_*$ alone.

Figure 4 displays geometric optical depth profiles $\tau_\perp(r)$. As expected from our analysis in § 3.2, disks separate into two types, CPR-dominated type A and collision-dominated type B. As $\dot{M}_*$ increases, disk behavior changes from type B to type A. One consequence is that the inner disk becomes increasingly filled in. Furthermore, for type A disks, we expect $\tau_\perp \propto r^{-5/2}$ at $r \gg r_{BR}$; this behavior is indeed evident for $\dot{M}_*/\dot{M}_\odot \in (10^2, 10^3)$. For type B disks, we expect $\tau_\perp \propto r^{-3/2}$ at $r \gg r_{BR}$; the models for which $\dot{M}_*/\dot{M}_\odot \in (1, 10)$ exhibit this scaling.

FIG. 7.—Color profile (F606W $- H$) computed using our theoretical Monte Carlo model. Solid, dashed, dot-dashed, and double-dot–dashed curves correspond, respectively, to $\dot{M}_*/\dot{M}_\odot = \{1, 10, 10^2, 10^3\}$. The vertical dotted line corresponds to $r_{BR} = 43$ AU, the radius of the birth ring containing dust-producing parent bodies; the horizontal dotted line is the star's color. The outer disk is expected to be bluer in scattered near-infrared light than the inner disk.
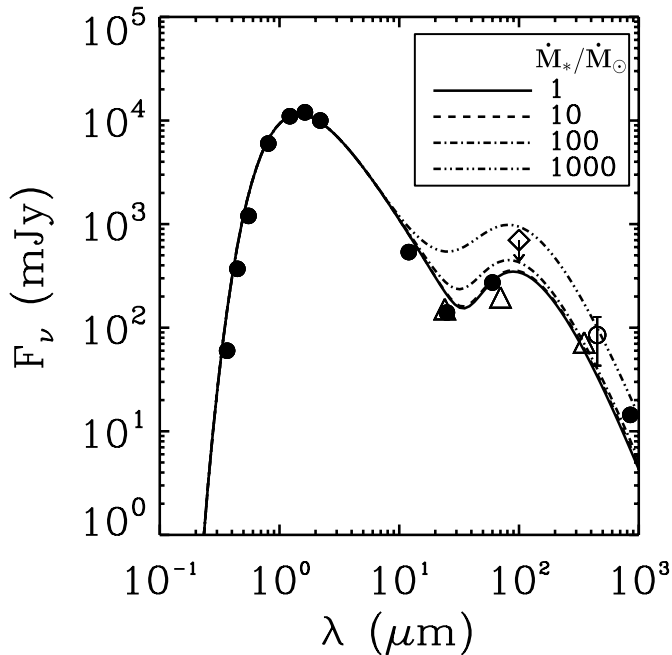
Fig. 8.—Spectra computed using our theoretical Monte Carlo model. Solid, dashed, dot-dashed, and double-dot–dashed curves correspond, respectively, to $\dot{M}_*/\dot{M}_\odot = \{1, 10, 10^2, 10^3\}$. Data from Liu et al. (2004; *circles and diamond*) and Chen et al. (2005; *triangles*) are overlaid; the open circle is a possible detection, and the diamond represents an upper limit. The discrepancy between theory and observation at $\lambda \approx 12$ μm is due to our use of a blackbody spectrum for the central M dwarf; better agreement can be had by employing more realistic stellar atmosphere models (e.g., Allard et al. 2001). The discrepancy at the longest wavelengths between the data and the law-$\dot{M}_*$ models is due at least in part to the fact that the maximum grain size in our simulations is $500s_{blow} \ll s_{max}$; were we to increase the number of particles J in our simulation, the discrepancy would be reduced.

We compare our theoretical surface brightness profiles SB(b) with data from K05 in Figures 5 and 6, for the cases of high $\dot{M}_*$ and low $\dot{M}_*$, respectively. For all disk models, there is a significant contribution to the surface brightness at $b < r_{BR}$ from starlight that is forward scattered by grains located within the half of the birth ring nearest the observer. As $\dot{M}_*$ increases, the inner disk fills in and the surface brightness at $b < r_{BR}$ increases. In comparison, the surface brightness at $b \gg r_{BR}$ decreases with increasing $\dot{M}_*$, reflecting the transition from the $\tau_\perp \propto r^{-3/2}$ scaling of type B disks to the $\tau_\perp \propto r^{-5/2}$ scaling of type A disks. Examination of either the inner or outer disk profiles reveals that models for which $\dot{M}_*/\dot{M}_\odot \in (1, 10)$ fit the data better than do models for which $\dot{M}_*$ is higher. Discrepancies between these low-$\dot{M}_*$ models and the observations are less than a factor of 2. They might arise in part from our use of a scattering phase function (P) appropriate for idealized spherical grains of pure water ice.

In Figure 7 we plot $V - H$ colors. For low values of $\dot{M}_*$, the inner disk is largely evacuated and so there is little variation in color with b for $b < r_{BR}$. The outer disk becomes progressively bluer with b as ever smaller (still bound) grains are probed. All of these trends are in agreement with observations of disk color (S. Metchev 2005, private communication; M. Fitzgerald 2005, private communication).

In Figure 8 we plot our theoretical spectra together with flux measurements from Liu et al. (2004) and Chen et al. (2005). The filled inner disks of high-$\dot{M}_*$, type A models produce too much emission at mid-infrared wavelengths to compare well with observations. As was our conclusion from studying the surface brightness profile in reflected starlight, the thermal emission spectra point to stellar mass-loss rates of $\lesssim 10\dot{M}_\odot$.

5. SUMMARY AND DIRECTIONS FOR FUTURE WORK

We have constructed a theory to explain the observed optical surface brightness profile and infrared emission spectrum of the debris disk encircling AU Mic. In our theory, the slope of surface brightness versus projected radius b changes abruptly at $b = 43$ AU because a birth ring of planetesimals exists at stellocentric radius $r = r_{BR} = 43$ AU. This ring has a full radial width $\Delta r \sim 0.1 r_{BR}$ and a vertical, geometric optical depth of $\tau_{\perp, BR} \sim 0.004$. The parent bodies in the ring have sizes $s_{max} \sim 10$ cm and a total mass of $M_{max} \sim 0.01$ $M_\oplus$. Collisional attrition of parent bodies generates micron-sized grains that scatter starlight at optical wavelengths. The population of visible grains is maintained in steady state: production by colliding parent bodies balances removal by grain-grain collisions and removal by corpuscular and Poynting-Robertson (CPR) drag. The timescales over which removal of visible grains occurs can be orders of magnitude shorter than the age of the system (~ 12 Myr), ensuring steady state.

Collisions between parent bodies initiate a collisional cascade that extends downward in particle size by several orders of magnitude. Grains having sizes $s < s_{blow} \approx 0.2$ μm are expelled from the system by stellar wind and radiation (SWR) pressure and contribute negligibly to the observed optical emission. Instead, barely bound grains, having sizes just larger than s_{blow} and which occupy highly eccentric orbits, make the dominant contribution to the surface brightness in the outer disk at $r > r_{BR}$. The number of such grains rises more steeply than would be expected from a pure Dohnanyi size spectrum as s approaches s_{blow} from above because grains on high-eccentricity orbits have prolonged lifetimes against CPR drag and collisions. The structure of the outer disk depends on whether these smallest of bound grains are removed principally by CPR drag (type A conditions) or by destructive grain-grain collisions (type B conditions). As the luminosity and/or mass-loss rate of the central star increase, disk behavior grades from type B to type A. As the number of parent bodies in the birth ring increases, collision rates increase and disk behavior changes from type A to type B. In the outer reaches of type A disks, the vertical optical depth scales approximately as $\tau_\perp \propto r^{-5/2}$. Under type B conditions, $\tau_\perp \propto r^{-3/2}$ (but see footnote 7). We have derived these scaling relations analytically and have verified them by Monte Carlo simulations.

The inner regions at $r < r_{BR}$ are populated by grains that survive long enough before suffering destructive collisions that their periastron distances diminish appreciably by CPR drag. In type A disks, a significant fraction of grains born in the birth ring meet this criterion, so the inner disk is characterized by the same vertical optical depth that characterizes the birth ring. By contrast, under type B conditions, the inner disk is practically empty.

In the case of AU Mic, type B conditions prevail. By fitting simultaneously both the surface brightness profile and the thermal emission spectrum, we not only uniquely determine the vertical optical depth and radial width of the birth ring (see the values cited above) but also constrain the stellar mass-loss rate $\dot{M}_*$ to be $\lesssim 10\dot{M}_\odot$. According to our theory, the inner disk of AU Mic at $r < r_{BR}$ is empty. The observed surface brightness at $b < r_{BR}$ is not zero because we are observing the disk edge-on. The primary contribution to the surface brightness at $b < r_{BR}$ arises from starlight that is forward scattered by grains in the birth ring.

Our theory states that the observed structure of the AU Mic disk reflects processes that are balanced in steady state. Equilibrium is likely since the timescales over which collisions and CPR drag operate, even in the rarefied outer disk, are shorter than the age of the system. The outer disk does not comprise

"primordial" grains left behind from a now-evaporated gaseous disk, as has been speculated previously. Nor is the manifestation of the debris disk phenomenon in AU Mic the outcome of a recent cataclysm that has not yet equilibrated. That our required parent body mass is modest (eq. [42]) supports our contention that the AU Mic disk is in steady state.

As our paper was being completed, we became aware of an independent study of AU Mic by Augereau & Beust (2006). These authors find, by inverting the observed surface brightness profile, that the underlying vertical optical depth of the AU Mic disk peaks near 35 AU. It is heartening that their conclusion is consonant with one of ours, derived as they are using complementary approaches: detailed data-fitting procedures versus physical reasoning to understand dust dynamics under general circumstances.

The ring of parent bodies at $r_{BR} = 43$ AU that we envision encircling AU Mic presents a youthful analog to the solar system's Kuiper Belt (see Chiang et al. 2006). The spatial dimensions of these systems are remarkably similar: the classical Kuiper Belt, containing those planetesimals thought to have formed in situ, extends in heliocentric distance from ~40 to ~47 AU (e.g., Trujillo & Brown 2001).

We conclude by pointing out directions for future work on AU Mic and other debris disks:

1. *Disk thickness.*—By assuming that we are viewing the AU Mic disk perfectly edge-on, we estimated a full disk height of $h_{BR} \approx 2.75$ AU. The corresponding opening angle is $h_{BR}/r_{BR} \approx 4°$. While our model of a type B disk succeeds in reproducing the observed scaling behavior of disk height ($h \propto b^0$ in the inner disk and $h \propto b^1$ in the outer disk), we have not explained what sets the normalization. Dissipative grain-grain collisions would be expected to damp the inclination dispersion and to reduce h_{BR} to values orders of magnitude smaller than our inferred value.

2. *Application to other systems.*—The debris disk surrounding the A star β Pictoris closely resembles the AU Mic disk (Liu 2004). The surface brightness profile abruptly changes slope at $b \approx 100$ AU, from SB $\propto b^{-2.4}$ to SB $\propto b^{-4.0}$ (Kalas & Jewitt 1995). Moreover, the vertical scale height h scales with b the same way that it does in the AU Mic disk.[10] Recently, another analog to

the AU Mic disk has been discovered: F star HD 139664 hosts a debris disk whose surface brightness profile exhibits a sharp break at ~90 AU (Kalas et al. 2006). The theory we have laid out for AU Mic might find ready application to these other systems.

3. *Uniqueness of AU Mic among M dwarfs.*—The pioneering Keck survey conducted by PJL05 at $\lambda = 11.7$ μm reveals that AU Mic is distinguished among their sample of nine M dwarfs having ages of 10–500 Myr in emitting an infrared excess. Why? Do the other M dwarfs not possess disks? As M dwarfs constitute the most numerous stars in the universe, understanding why AU Mic might be exceptional will help to determine the prevalence of planetary systems. Many of the M dwarfs surveyed by PJL05 may simply be much older than AU Mic; their parent body populations may have suffered near complete comminution.

4. *Ubiquity of rings.*—That parent bodies are confined to a ring centered at 43 AU in the AU Mic system calls for explanation. Ring morphologies are so common—witness the examples of HR 4796A (Schneider et al. 1999), ϵ Eridani (Greaves et al. 1998), Fomalhaut (Kalas et al. 2005), and even the Kuiper Belt—that the "debris disk phenomenon" might well be more precisely termed the "debris ring phenomenon." While regions interior to rings might have been purged of material by planets, the physical processes that determine the outer edges of rings remain unclear. Ideas proposed by Takeuchi & Artymowicz (2001) and Klahr & Lin (2005) for how interactions between solids and gas can concentrate planetesimals into rings might be relevant. That planetary systems have sharp outer edges suggests that planetesimal formation is not a continuous function of disk properties; rather, the formation of planets may require disk properties to meet threshold conditions (e.g., Youdin 2004).

[10] That the color of β Pic's outer disk is red rather than blue (by contrast to the case of AU Mic) could be a consequence of the particular grain size required for blowout in the β Pic system, since for certain grain sizes and compositions $Q_{scat}(\lambda, s)$ can actually increase with increasing wavelength. See Bohren & Huffman (1983) for a discussion of this phenomenon of "blueing."

REFERENCES

Allard, F., Hauschildt, P. H., Alexander, D. R., Tamanai, A., & Schweitzer, A. 2001, ApJ, 556, 357
Artymowicz, P. 2000, Space Sci. Rev., 92, 69
Augereau, J.-C., & Beust, H. 2006, A&A, in press (astro-ph/0604313)
Augereau, J.-C., Nelson, R. P., Lagrange, A. M., Papaloizou, J. C. B., & Mouillet, D. 2001, A&A, 370, 447
Aumann, H. H., et al. 1984, ApJ, 278, L23
Bohren, C. F., & Huffman, D. R. 1983, Absorption and Scattering of Light by Small Particles (New York: Wiley)
Burns, J. A., Lamy, P. L., & Soter, S. 1979, Icarus, 40, 1
Campo Bagatin, A., Cellino, A., Davis, D. R., Farinella, P., & Paolicchi, P. 1994, Planet. Space Sci., 42, 1079
Chen, C., et al. 2005, ApJ, 634, 1372
Chiang, E. I., Joung, M. K., Creech-Eakman, M. J., Qi, C., Kessler, J. E., Blake, G. A., & van Dishoeck, E. F. 2001, ApJ, 547, 1077
Chiang, E. I., Lithwick, Y., Murray-Clay, R., Buie, M., Grundy, W., & Holman, M. 2006, in Protostars and Planets V, ed. B. Reipurth, D. Jewitt, & K. Keil (Tucson: Univ. Arizona Press), in press (astro-ph/0601654)
Dohnanyi, J. S. 1969, J. Geophys. Res., 74, 2531

Fujiwara, A., Cerroni, P., Davis, D., Ryan, E., & di Martino, M. 1989, in Asteroids II, ed. R. P. Binzel, T. Gehrels, & M. S. Matthews (Tucson: Univ. Arizona Press), 240
Goldreich, P., Lithwick, Y., & Sari, R. 2004, ARA&A, 42, 549
Greaves, J. S., Wyatt, M. C., Holland, W. S., & Dent, W. R. F. 2004, MNRAS, 351, L54
Greaves, J. S., et al. 1998, ApJ, 506, L133
Greenberg, R., Hartmann, W. K., Chapman, C. R., & Wacker, J. F. 1978, Icarus, 35, 1
Habing, H. J., et al. 2001, A&A, 365, 545
Housen, K. R., & Holsapple, K. A. 1990, Icarus, 84, 226
Hünsch, M., Schmitt, J. H. M. M., Sterzik, M. F., & Voges, W. 1999, A&AS, 135, 319
Kalas, P., Graham, J. R., & Clampin, M. 2005, Nature, 435, 1067
Kalas, P., Graham, J. R., Clampin, M. C., & Fitzgerald, M. P. 2006, ApJ, 637, L57
Kalas, P., & Jewitt, D. 1995, AJ, 110, 794
Kalas, P., Liu, M. C., & Matthews, B. C. 2004, Science, 303, 1990
Klahr, H., & Lin, D. N. C. 2005, ApJ, 632, 1113

Krist, J. E., et al. 2005, AJ, 129, 1008 (K05)

Lagrange, A.-M., Backman, D. E., & Artymowicz, P. 2000, in Protostars and Planets IV, ed. V. Mannings, A. P. Boss, & S. S. Russell (Tucson: Univ. Arizona Press), 639

Lecavelier des Etangs, A., Vidal-Madjar, A., & Ferlet, R. 1996, A&A, 307, 542

Liu, M. C. 2004, Science, 305, 1442

Liu, M. C., Matthews, B. C., Williams, J. P., & Kalas, P. G. 2004, ApJ, 608, 526

Magee, H. R. M., Güdel, M., Audard, M., & Mewe, R. 2003, Adv. Space Res., 32, 1149

Metchev, S. A., Eisner, J. A., Hillenbrand, L. A., & Wolf, S. 2005, ApJ, 622, 451

Meyer, M. R., Backman, D. E., Weinberger, A. J., & Wyatt, M. C. 2006, in Protostars and Planets V, ed. B. Reipurth, D. Jewitt, & K. Keil (Tucson: Univ. Arizona Press), in press (astro-ph/0606399)

Murray, C. D., & Dermott, S. F. 1999, Solar System Dynamics (Cambridge: Cambridge Univ. Press)

O'Brien, D. P., & Greenberg, R. 2003, Icarus, 164, 334

Pan, M., & Sari, R. 2005, Icarus, 173, 342

Parker, E. N. 1964, ApJ, 139, 93

Plavchan, P., Jura, M., & Lipscy, S. J. 2005, ApJ, 631, 1161 (PJL05)

Roberge, A., Weinberger, A. J., Redfield, S., & Feldman, P. D. 2005, ApJ, 626, L105

Schneider, G., et al. 1999, ApJ, 513, L127

Schrijver, C. J., & Title, A. M. 2001, ApJ, 551, 1099

Smith, B. A., & Terrile, R. J. 1984, Science, 226, 1421

Song, I., Zuckerman, B., Weinberger, A. J., & Becklin, E. E. 2005, Nature, 436, 363

Strassmeier, K. G. 2002, Astron. Nachr., 323, 309

Su, K., et al. 2005, ApJ, 628, 487

Takeuchi, T., & Artymowicz, P. 2001, ApJ, 557, 990

Telesco, C. M., et al. 2000, ApJ, 530, 329

Torres, C. A. O., & Ferraz Mello, S. 1973, A&A, 27, 231

Trujillo, C. A., & Brown, M. E. 2001, ApJ, 554, L95

Warren, S. G. 1984, Appl. Optics, 23, 1206

Weber, E. J., & Davis, L. 1967, ApJ, 148, 217

Wood, B. E., Müller, H.-R., Zank, G. P., & Linsky, J. L. 2002, ApJ, 574, 412

Wood, B. E., Müller, H.-R., Zank, G. P., Linsky, J. L., & Redfield, S. 2005, ApJ, 628, L143

Wyatt, M. C. 2005, A&A, 433, 1007

Wyatt, S. P., & Whipple, F. L. 1950, ApJ, 111, 134

Youdin, A. N. 2004, in ASP Conf. Ser. 323, Star Formation in the Interstellar Medium: In Honor of David Hollenbach, ed. D. Johnstone et al. (San Francisco: ASP), 319

Zuckerman, B. 2001, ARA&A, 39, 549

Zuckerman, B., & Song, I. 2004, ApJ, 603, 738